Degree Project in Chemistry , 30 Credits
Stockholm, Sweden 2022

Reaction of Copper and Copper(I) Iodide with Iodine and Strong Field Ligands

Supervisor: Professor James Gardner

Co-Supervisor: Mahboubeh Jamshidisemirom

Student: Aya Ali

Table of Contents

Abstract

Perovskite solar cells (PSCs) are known as light-harvesting devices with increased power conversion efficiencies (PCE). PSCs are known for their flexibility and high tolerance towards defects. It consists of five different layers with different materials and functions. Transparent electrode, electron transport layer (ETL) , perovskite or active layer , hole transport layer (HTL) and metallic electrode. In this research project, the focus is directed towards the metallic electrode (Cu-thin film), hole transport layer (CuI-thin film) and the active layer (CuI-complex). The purpose of this study is to investigate the effect of different thicknesses on the surface morphology and roughness and to see how much iodine is diffusing through the film by calculating the volume.

The results of this project present that the increase in thickness leads to an increase in roughness. It also shows that an increase in thickness leads to a more homogeneous and uniform surface and in addition the grain size increases which indicates that the quality of crystallization improves. Finally, by knowing the thickness and surface area of the samples the volume was calculated to indicate how much iodine is diffusing through the film and the results for this part indicated that the thicker the sample, more iodine will diffuse through the film.

Sammanfattning

Perovskit solceller (PSCs) är kända som 'ljusomvandling' enheter med ökad omvandlingseffektivitiet (PCE). PSCs är kända för detta flexibilitet och hög tolerans mot defekter och består av fem lager med olika material och egenskaper. De fem lagren är följande; transparant elektrod, elektron ledande lager (ETL), perovskit lager, hål ledande lager (HTL) och metallelektroden. Detta forskningsarbete fokuserar på metallelektroden (Cu-tunn film), HTL (CuI-tunn film) och det aktiva lagret (CuI-komplex). Syftet med denna studie är att undersöka effekten av olika tjocklekar på ytans morfologi och grovhet för att se mängden jod som tränger sig genom filmen genom att beräkna volymen.

Resultatet av denna studie visar att ökad tjocklek leder till ökad grovhet. Man ser även att en ökad tjocklek leder till ett mer homogent och jämn yta, och dessutom ökar kornstorleken, vilket tyder på att kvaliten av kristallisationen förbättras. Slutligen, genom att känna till tjockleken och storleken (arean) på ytan av proverna kunde man beräkna volymen för att indikera mängden jod som trängt sig genom filmen. Resultatet av denna del indikerade att ju tjockare provet är, desto mer kommer jod att tränga sig genom filmen.

1. Introduction

According to BP Statistical Review of World Energy 2022, approximately 84% of the world's consumption for energy is met from fossil fuel [1]. For more than a century fossil fuels such as crude oil, coal and natural gas have been used to generate the energy required to propel different transportation , produce electricity in large power stations and provide heat in households [2]. The most used fossil fuel is oil with a percentage of 33.05% of the total energy consumption along with coal and natural gas accounting for 27.3% and 24.2% respectively. Principally, the energy needed from fossil fuel is obtained through combustion of the fuel; however, fossil fuel combustion to release energy is considered one of the greatest contributors to increased levels of carbon dioxide (CO2) in the atmosphere. CO2 is a greenhouse gas which alters the earth ecosystem and increases the earth's average air temperatures by accumulating in the atmoshpere [2].

Besides releasing a greenhouse gas (CO2), the burning of fossil fuels has an effect on the environment in several ways. For instance the emitting of different pollutants such as sulfur dioxide which minimize air quality and cause respiratory issues. Moreover, combustion of fossil fuel generates airborne particles such as sulfate aerosols which increase the reflectivity of the atmosphere and cause a cooling effect. Airborne partickles also contribute to the melting of snow and ice in certain regions of the world. To be more specific, airborne particles (mostly soot) land on snow and due to their dark color, it increases the absorption of sunlight which leads to surface heating and finally snow melting. This phenomena has an effect on the local patterns of freshwater availability [3].

Due to all the previous effects, the key to a sustainable development is to replace fossil fuel with renewable energy sources. In recent years there has been considerable attention towards the development of renewable energy which allows fuel diversification and provides reliable supplies of power, therefore it strengthens energy security, protects the nation's natural sources and reduces the risk on the environment. These sources have a positive impact in many sectors, it leads to the development of the economic sector and minimizes the global risks related to climate change .

Moreover, one of the most sustainable and abundant renewable resources is solar energy, often called clean energy. The generation of solar radiation or light energy in the sun happens as a result of nuclear fusion reactions and by the help of electromagnetic radiation in quanta, it is transmitted into the earth. Solar energy is abundant meaning it will never run out or be in short supply. In addition, to describe the abundance of solar energy, if for instance 1% of the Sahara desert is covered with solar panels, it could generate sufficient electricity for the whole world [4][5].

1.1 Background

As mentioned previously, global energy consumption and environmental pollution are considered serious threats to the ecosystem. To rival the consumption of fossil fuel, solar energy must be used in a cost-effective way. There are different types of solar cells that use different materials for each layer. The most known one on the market is silicon solar cells with an increased power conversion efficiency (PCE) from 12 % to 25 % over the years [6]. It is characterized by the long lifetime up to 20 years and the cheap production price; however, the manufacturing process demands a large amount of heat energy, specifically in the production of crystalline silicon structures. Additionally, it demands the use of toxic and rare materials such as cadmium telluride, silicon tetrachloride and copper indium selenide which can lead to device degradation [7]. Therefore, researchers are searching for other reliable materials that mostly come from organic and abundance materials to be employed in structured solar cells such as organic, dye-sensitized, and perovskite solar cells (PSCs).

Among the different types of solar cells, PSCs exhibit the greatest power conversion efficiency (PCE) from 9.7% to 22% over a period of five years. However, during operation PSCs can lose their efficiency due to different factors. PSCs is considered an attractive area of research due to several reasons: The manufacturing process is cheaper and does not require a large amount of heat energy, it is simpler to apply different layers by the use of simple techniques such as spin coating and it can be fabricated into flexible surfaces [8].

The first perovskite solar cells were introduced in 2009 and had low stability due to liquid electrolyte that damages the perovskite layer and electrodes while operating. It was also characterized with a low conversion power of only 3.8%. Since then , researchers have put great effort into improving their performance [9].

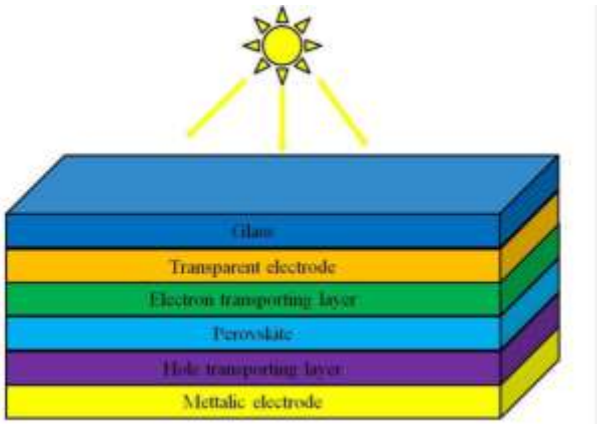

Figure (1): schematic structure of perovskite solar cell

Figure 1, describes the general structure of PSCs with different five layers. Starting from the top, it consists of a glass surface and below this glass there is a transparent electrode such as fluorine doped tin oxide (FTO) or indium tin oxide (ITO). The ITO/FTO is connected to the electron transporting layer (ETL) and next there is the perovskite layer which is defined as the active layer where the absorption of light photons and the electron-hole pair excitation is happening. Moving from the perovskite layer, there is hole transport layer (HTL) which is responsible for hole extraction and transport. Moreover, the final layer is a metallic electrode which is connected to the transparent electrode in order to create a closed circuit cell. Throughout the years, much research and development was made on all the layers in the solar cell structures due to their contribution to the total PCE [10].

1.2 PhotoVoltaic effect:

Photovoltaic effect (PV), is defined as the principle of generating electricity through solar radiation. This effect arises when sunlight strikes a semiconducting material in which the illuminated photons of the light have equal or higher energy than the semiconductor's energy gap. The energy gap is defined as the differences in energy between the valence band and the conduction band. The valence band consist of the highest energy bonding orbitals for a semiconductor, on the other hand the conduction band is the energy level which will accept excited electrons. For molecular semiconductors these two levels are defined as HOMO-LUMO gap. Moreover, in order to excite electrons from the valence band/HOMO to the conduction band/LUMO a specific energy is required which can be determined by the material [10].

Light is described as the electromagnetic radiation which consists of photons with their specific energy. The energy of each photon depends on its wavelength with the following relation:

$$E = \frac{hc}{\lambda}$$

Where E is defined as the energy of a photon, C is the speed of light, h is plank constant and λ is the wavelength of the photon. Semiconductors can be excited by these photons. For instance, if the photon has an energy larger than the energy gap of the material, it will be absorbed which leads to the excitation of electrons in the valence band/HOMO to the conduction band/LUMO. This excitation of energy will leave holes in the valence band/HOMO. Furthermore, the excited electron and the holes left behind want to recombine, however instead of recombining, the charge carrier will be diffused due to the electric field built up by the opposite electrodes. Current is produced by the movement of these charge carries and voltage is created by the material band gap [10].

1.3 Aim of work

The purpose of this research project is to synthesize three layers of solar cell which are metallic electrode, HTL and absorbent layer and to investigate the effect of different thicknesses on the surface morphology and roughness. Moreover, the diffusion of iodine through the film is determined by calculating the volume of CuI and CuI-ligand samples.

2. Experimental and Analytical Techniques

2.1 Experimental methods

2.1.1 Thermal evaporator

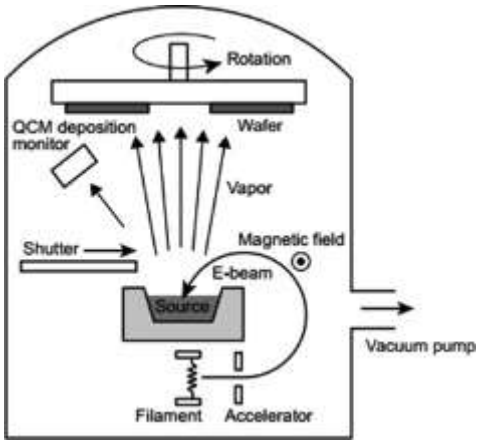

Figure (2): schematic diagram of thermal evaporator

Thermal evaporation using electron beam is a type of physical vapor deposition technique (PVD) which is known for a high deposition rate from 0.1 μm/min to 100 μm/min.This techniques is useful in terms of controlling the thin film morphology and structure with desired qualities such as the dense of the coating, low contamination and high productivity and reliability. The evaporation source (titanium and copper pellets) is heated directly under vacuum by electrons in the form of an intense electron beam which leads to the deposition of the vaporized material at the substrate to create a thin film [11]. The drawback of this technique is that it is time consuming however, it produces stable thin film that can last for several months.

2.1.2 Electroless plating of copper

Electroless plating is a nonelectric technique of depositing copper thin film from solution. The plating bath should contain a metal salt which is copper sulfate, and an appropriate reducing agent which is paraformaldehyde. There are pre-surface treatment steps before dipping the sample into the copper bath. The sample should be treated with tin chloride solution to improve the wettability and adhesion of the surface and then dipped into a catalytic solution of palladium chloride to create a catalytic site on the surface and finally into the copper bath where the thin film will form within 3-5 minutes [12]. This method is simple and fast compared to the thermal evaporator; however, the produced thin film is not stable and can evaporate within a few days.

2.1.3 Vapor iodination method

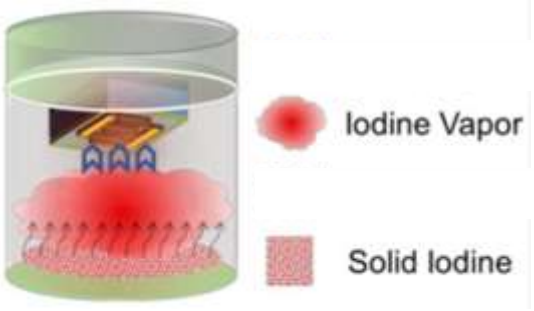

Figure (3): schematic diagram of iodination method

There have been several reported techniques for the synthesis of copper iodide (CuI) thin film such as pulsed laser deposition, magnetron sputtering and successive ionic layer adsorption and reaction (SILAR). However, these methods demand high temperatures and complex experimental procedures. Therefore, one of the most common and simple methods used to prepare CuI thin film is the iodination method. This method involves a chemical reaction between copper and iodine vapor [13].

Additionly, the same principle has been used to produce CuI complexes, CuI was placed inside a small vial which is placed inside a bigger one. 5-7 drops of 3,5-Dimethylpyridine was placed inside the larger vial. The vial was closed tightly and left for 24 hours.

2.2 Analytical techniques

2.2.1 Atomic force microscopy (AFM)

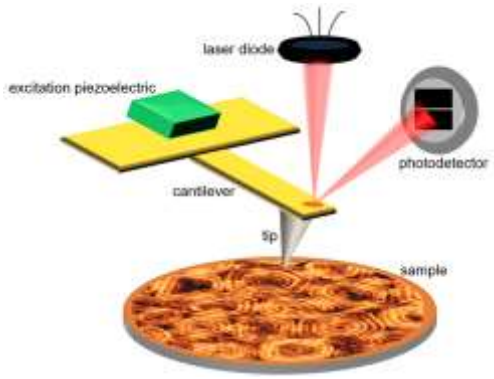

Figure (4): schematic diagram of AFM

Atomic force microscope (AFM) is an advanced high resolution scanning probe microscopy which operates on the principle of surface sensing. It uses a sharp tip to scan the sample surface line by line. As this tip approaches the surface, the cantilever starts to bend and this bending is recorded by the laser diode and split photodetector. When the tip is pressed into the surface sample and starts scanning, this motion is captured which creates the three dimensional image of the surface [14]. AFM in this project, is used to study the surface morphology, it provides information about the surface thickness and roughness.

2.2.2 X-Ray Diffraction (XRD)

X-ray diffraction analysis (XRD) is a technique used to determine phase identification of a crystalline material. It can additionally give information about unit cell dimensions, crystal size and structure. This technique uses x-ray beams because their wavelength is kind of similar to the spacing between the atoms in the sample. The x-ray beam passes through the sample and then it changes the direction at a specific angle from the original beam. This is known as the angle of diffraction. In this study, XRD is used to ensure the presence of Cu and CuI in our samples [15].

3. Synthesis of Copper thin film

3.1 Introduction

Despite the fact that PSCs have shown improvement in their PCE, reaching long term stability is still considered a challenge. In comparison to the different parts of PSCs, the electrodes layers which are considered equally important to the other functional layers have attracted less attention and the majority of efforts were directed towards ETL, HTL and perovskite layers. Moreover, it was proven that the instability of the metallic and transparent electrodes can lead to device degradation, therefore choosing a suitable material could increase the stability of the device [16].

Generally, there are two electrodes in PSCs, the main purpose of the electrodes is to collect holes and electrons from hole transport layer (HTL) and electron transport layer (ETL). Metals are employed usually as the back electrode due to several reasons. Metals have light reflectivity and high conductivity. On the other hand, the front electrode often consists of transparent conductive oxide such as fluorine doped tin oxide (FTO) or indium tin oxide (ITO). Both materials are considered sufficiently stable. In this research study, the focus is pointed towards the metallic electrode [17].

Until now, gold (Au) is used in many reported stable PSCs as the back electrode due to its limited reactivity which leads to higher efficiencies and stable devices. However, gold is considered one of the noble metals which means its unaffordable for a scalable production [17]. Additionally, specefic studies have found out that Au migrates from the electrode to the hole transport layer and perovskite layer until it reaches the front contact. As a result of this migration, there is a loss of efficiency which leads to device degradation [18].

Furthermore, the suitable material to be used as the back electrode would be a metal that does not interact with the absorbent layer and has high conductivity. Copper (Cu) is considered a good candidate because it is cheaper when compared to gold and it was mentioned in specific literature that in direct contact with the perovskite layer, copper is stable and does not interact. Additionally, there was no sign of diffusion of copper ions into internal layers of the solar cell. Therefore, copper thin film was used as the metallic back electrode [19].

3.2 Synthesis of thin film

Copper thin film was deposited on two different substrates (glass and silicon wafer) using a thermal evaporator. First, in order to remove any particles, grease and oil from the surface, the substrates were cleaned using RBS solution along with acetone and ethanol for 30 minutes in an ultrasonic bath, afterwards the substrate was dried with nitrogen gas. The starting material is titanium powder, the thickness of the deposited titanium thin film is 5 nm and it acts as an adhesion layer. In addition, a metallic copper was placed in a tungsten boat inside the chamber, the purity of copper was 99.98%. Two different thicknesses were obtained.

3.3 Results and discussions

3.3.1 Thickness of the thin film

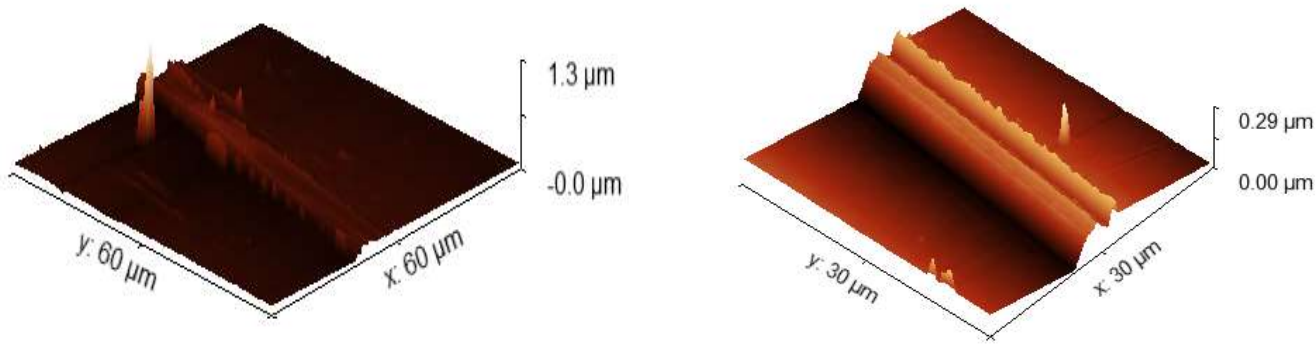

Figure (5): AFM images of copper thin film

An important factor in this project is the thickness of the thin film which will be used later to estimate the diffusion of iodine through the film. In order to measure the thickness of the thin film accurately, atomic force microscopy (AFM) was used to scan the area between the etched part and the thin film part. At the beginning, part of the substrate is masked with a paste to preserve it from the etching solution and a small part was etched with ferric chloride (FeCl3) solution. The etching solution consists of 4 grams of FeCl3 dissolved in deionized water. Figure 5, represents the differences in thickness between the thin film and the etched. By the use of gwyddion software, the average thickness was measured for both samples. The left image represents the 70 nm thin film and the right image represents the 140 nm thin film.

3.3.2 Morphology of the surface

a. **b.**

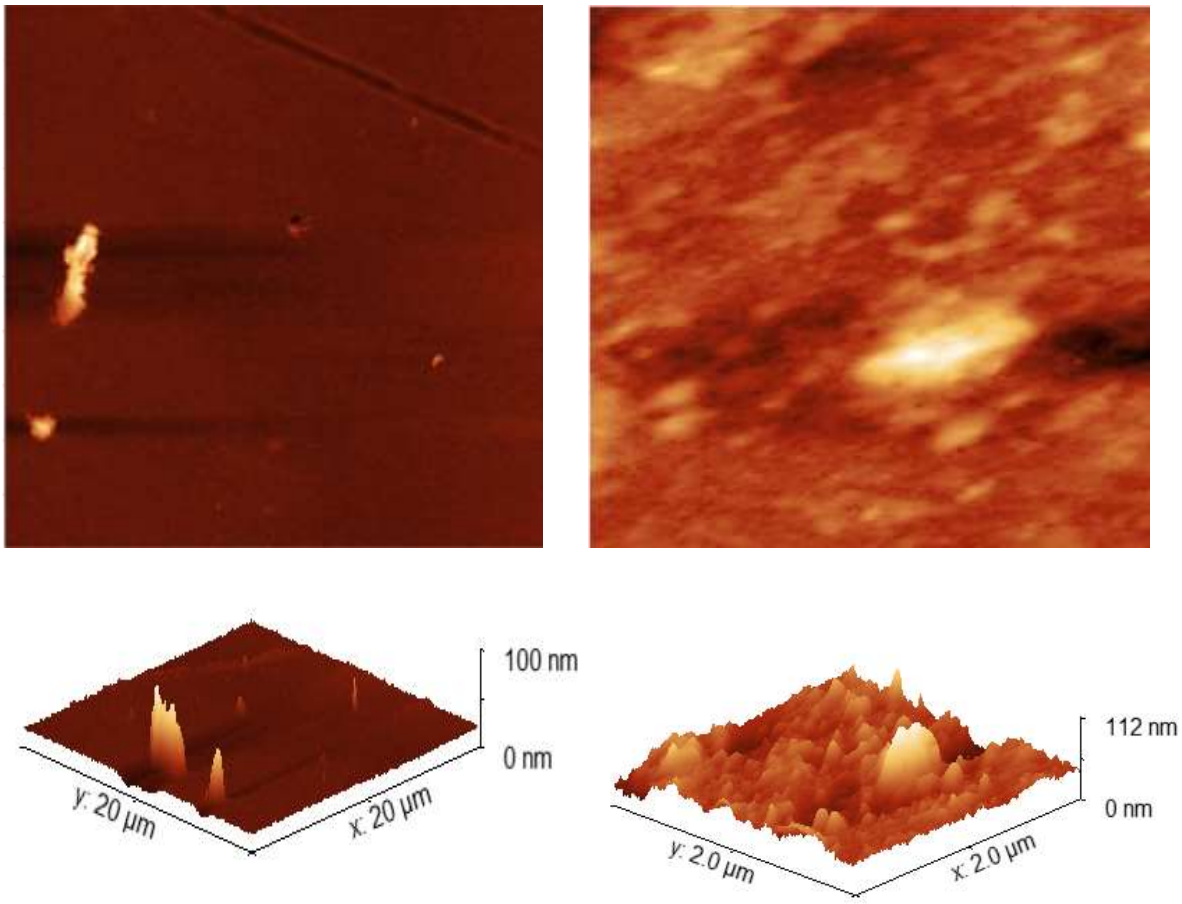

Figure (6): 2D and 3D AFM images of copper thin film

The surface topography and roughness were analyzed by atomic force microscopy (AFM) at room temperature. Figure 6, represents 2D and 3D images of copper thin film with two different thicknesses. To analyze the surface roughness, both mean roughness (Sa) and Root Mean Square (Sq) is measured by AFM. Sa is measured as the roughness average across the surface valleys and peaks. RMS is calculated as the root mean square of the surface valleys and peaks. The surface of the 70 nm film on the left has a mean roughness (Sa) of 1.3 nm along with RMS value of 4.8 nm. Whereas, the surface of the 140 nm film on the right shows an average roughness of 5.3 nm and RMS values of 10.85 nm. Therefore, It can be indicated from these values that the roughness has increased as the surface thickness increased from 70 to 140 nm and from observing the images it can be said that image a is smoother than b.

3.3.3 XRD Analysis

a. Thermal Evaporator Technique

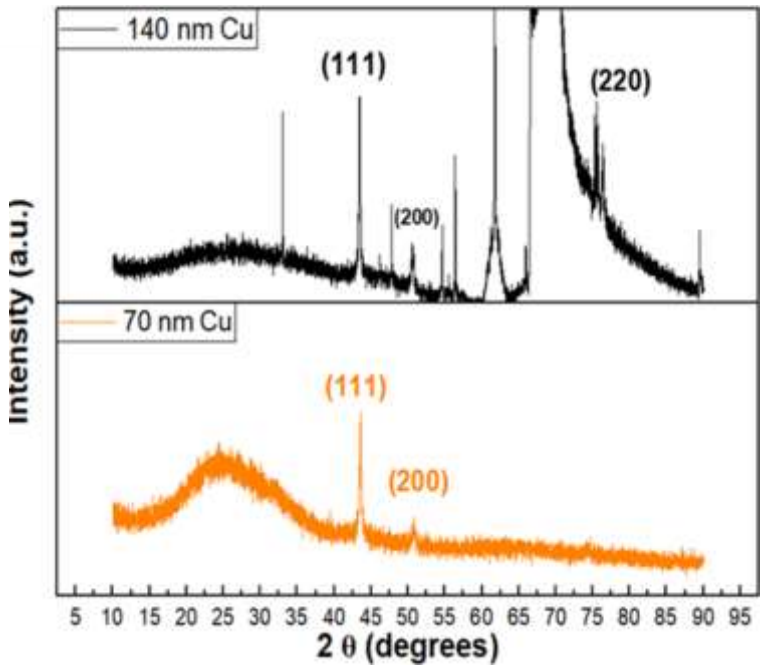

Figure (7): XRD pattern of Cu thin film with two different thicknesses

X-ray diffraction (XRD), was used in this project to study the structure and properties of the samples by analyzing their crystal structure. First it is confirmed that copper is present in the samples. Both thicknesses showed copper peaks around 43.3 and 50.5 which correspond to 111 and 200 respectively. For the thicker sample (140 nm), an additional peak related to copper is observed around 74.5 which corresponds to 220, this peak is missing from the 70 nm thin film. Moreover, it was observed that the intensities of the 111 and 200 copper peaks are higher for the thicker sample when it is compared to the 70 nm film. This indicates that as the thickness increases, the diffraction intensities of the peaks increases as well. This increase in thickness is beneficial to the improvement of crystallinity for copper thin films. The rest of the peaks correspond to silicon for the 140 nm film and the broadness at the beginning of the 70 nm pattern is due to the amorphous glass substrate.

b. Electroless Deposition Technique

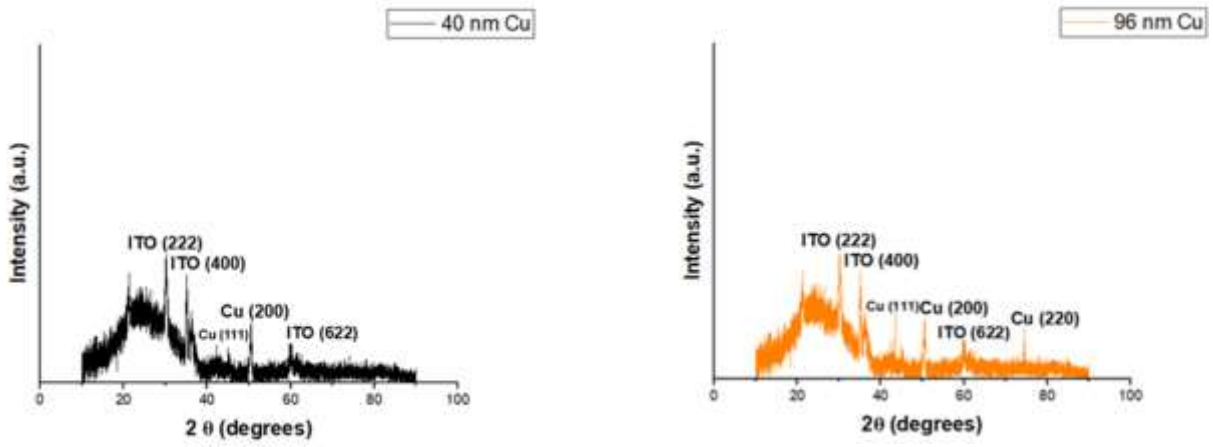

Figure (8): XRD pattern of Cu thin film with two different thicknesses

Moreover, for the electroless deposition method the thickness of the samples is indicated by the use of a profilometer and the thickness obtained corresponds to 40 nm and 96 nm thin film. XRD was employed again to check if the the results of the first part aligns with this part. First, there are several peaks which correspond to the ITO substrate but the focus is to check if copper peaks are present. For the 40 nm, a very small peak at 43.7 , a clear peak at 50.5 is observed and nothing around 74 , hence for the 40 nm sample two peaks of copper with relatively smaller intensities are observed. For the 96 nm film, weak but sharper peaks at 43.3 , 50.5 and 74.5 are observed in this sample indicating the presence of copper. Thus, for this method it is also concluded that the increase in thickness leads to an increase in diffraction intensities however, the intensities for this method are weak when compared to the samples obtained by the thermal evaporator.

4.Synthesis of Copper Iodide (CuI) thin film

4.1 Introduction

The hole transport layer (HTL) has several functions. For instance it can act as an energy barrier between the metal electrode and the perovskite layer which helps to prevent carrier recombination between the holes in the metallic electrode and electrons in the perovskite layer. Additionally, HTL can function as a metal ion diffusion barrier or moisture resistance layer which helps prevent device degradation [20].

Therefore, an ideal material for HTL should have specific properties such as high hole mobility, long-term stability and suitable energy level that match with the perovskite layer. Generally, there are two categories for hole transport materials (HTMs) which are organic and inorganic. In addition, PSCs that are based on organic HTMs have obtained high PCE however they have low mobility, limited conductivity and it was reported in various studies that in order to increase and modify the mobility and conductivity of organic HTMs, it has to be doped with toxic and hazardous dopants [20]. The toxic dopants could contribute to the device degradation. Thus, in this research copper iodide (CuI) is used for the HTL.

Zinc Blende copper iodide (CuI) is an inorganic semiconductor which has beneficial properties such as wide bandgap (3.1 eV at room temperature) which allows for a high transparency in the visible spectral range. Furthermore, it is considered a p-type semiconductor due to its high hole mobility (>40 cm2V−1·s−1in bulk) and it has an excitation binding energy up to 62 meV [21]. Additionally, due to its stable cubic structure, CuI can be synthesized at room temperature unlike other p-type transparent conductors (TCs) which require high temperatures. Furthermore, CuI consists of nontoxic and abundant elements and it can be synthesized with low cost using different deposition methods [21].

Different techniques have been reported to prepare CuI thin films such as successive ionic layer adsorption and reaction (SILAR), vacuum thermal evaporation , pulsed laser deposition , sputtering and vapor iodization [21]. In this paper, CuI thin film with different thicknesses have been prepared using vapor iodization.

4.2 Synthesis

Iodine vapor was deposited on Cu thin film which was prepared in the previous section with a simple procedure. 100 mg of CuI were placed inside a petri dish and copper thin film sample was fixed with a tape at the top to ensure complete exposure to iodine vapor. The procedure was done at 100◦C for 30 minutes. Afterwards, the samples were directly placed at the top of the hot plate for 10 minutes to ensure complete deposition.

4.3 Results and discussion

4.3.1 Thickness of the thin film

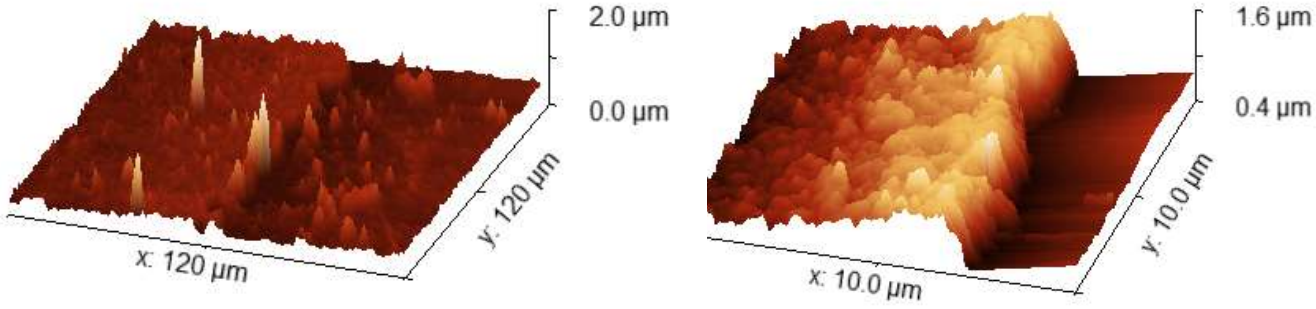

Figure (9): AFM 3D images of CuI samples with two different thicknesses

As mentioned before, thickness plays an important role in this study as it is one of the factors that determine the volume of CuI. The volume can indicate how much iodine is diffusing through the thin film. The previous steps were done here as well, part of the substrate is masked and the other part is etched. As expected, both samples showed a significant increase in thickness. The 70 nm sample has increased to 160 nm (left) and the 140 nm has increased to 270 nm (right).

In order to measure the volume which indicates the diffusion of iodine through the thin film, both values of lengths and width of the samples were taken and by knowing the thickness of each sample, the volume can be calculated using the following equation:

$$Volume\ (cm^3) = Length\ (cm) \times Width\ (cm) \times Thickness\ (cm)$$

Table 1: Dimensions values of both substrates

Sample	Length (cm)	Width (cm)	Thickness (cm)	Volume (cm^3)
160 nm CuI	1	0.8	0.000016	0.0000128
270 nm CuI	1	0.7	0.000027	0.0000189

Therefore, it can be concluded here that the thicker sample has a higher volume compared to the 160 nm CuI, which indicates more diffusion of iodine through the film.

4.3.2 Morphology of the surface

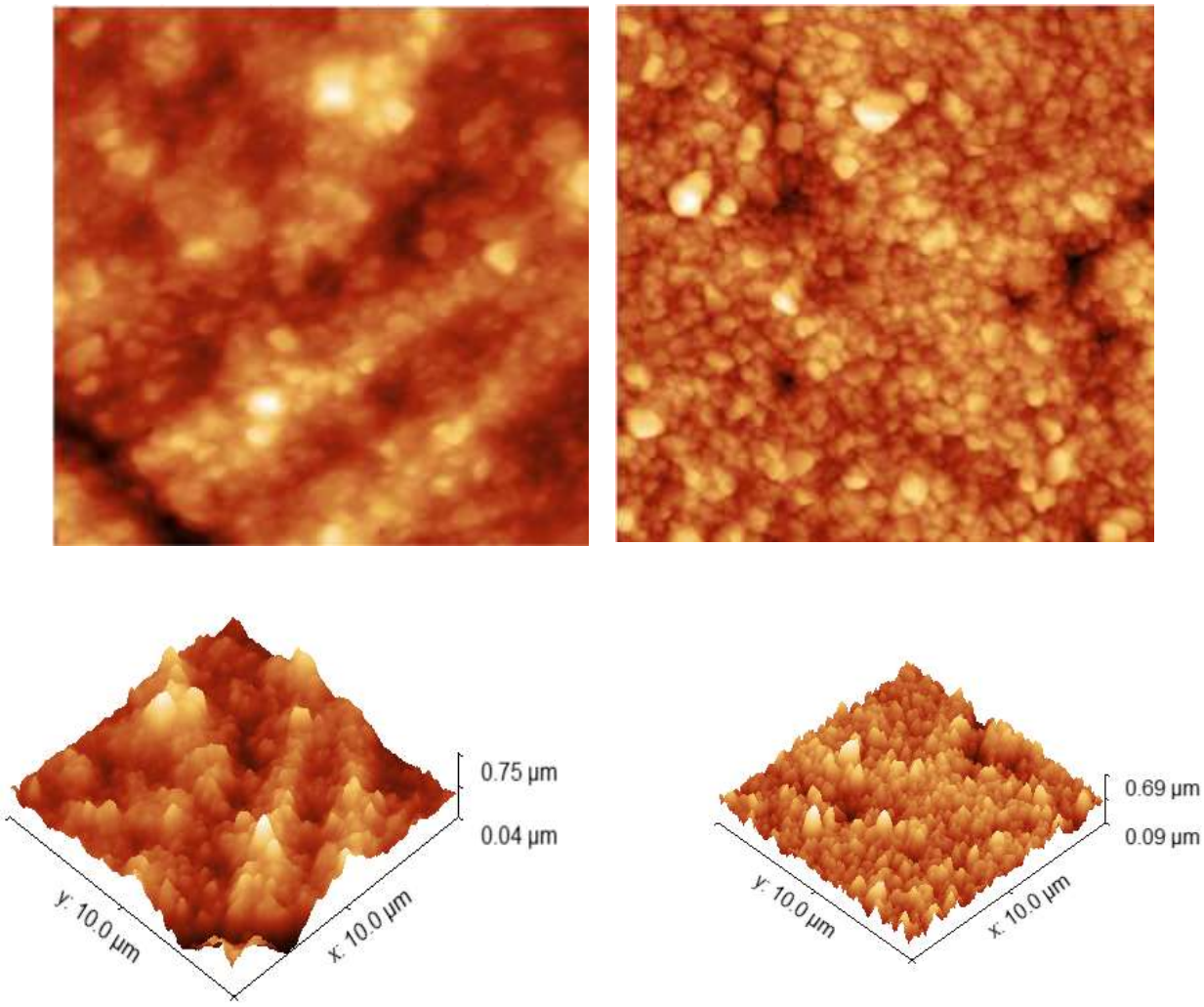

Figure (10): 2D and 3D AFM images of CuI

Figure 10, represents 2D and 3D images of CuI with two different thicknesses. The left image represents 160 nm CuI film and the right image represents the 270 nm CuI. Again, the values of mean roughness (Sa) and Root Mean Square (Sq) were taken. For the 160 nm sample, the surface roughness has increased significantly with an Sa value of 52.34 nm and RMS value of 83.47 nm. Moreover, the 270 nm sample shows an increase in roughness with an Sa value of 63.9 nm and RMS value of 89.3 nm. As it was indicated previously, the roughness increases with increasing thickness.

Moreover, the 3D images show the surface morphology for the two different CuI samples and it can be seen that the 160 nm CuI surface (left) is nonuniform which indicates that the

crystallinity is poor. Whereas for the 270 nm (right) the surface became well defined and smoother. Hence, it can be concluded here that increasing the thickness leads to a more homogenous surface. Additionally, by increasing the thickness, the grain size increases which indicate that the quality of crystallization improves.

4.3.3 XRD analysis

a. Thermal Evaporator Technique

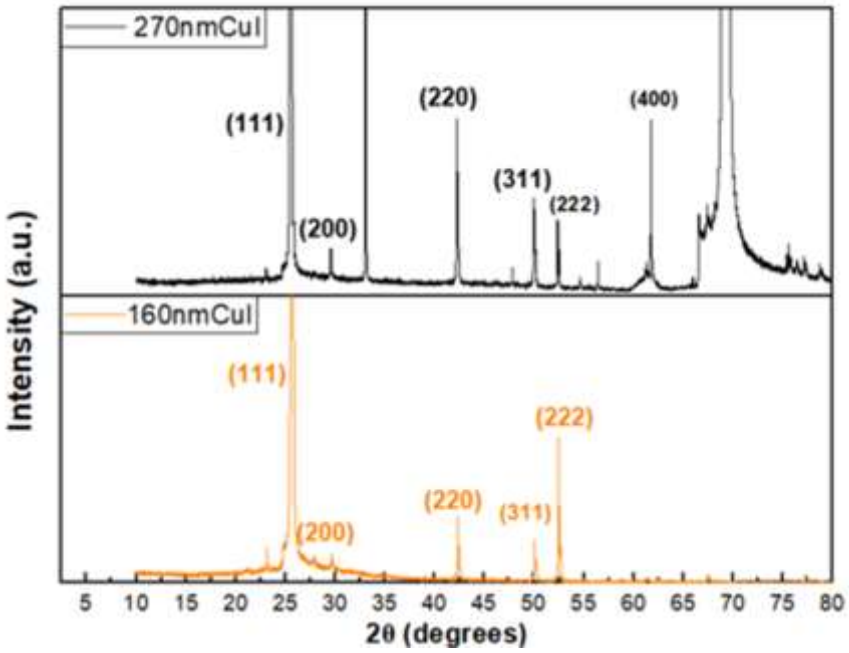

Figure (11): XRD pattern of CuI with two different thicknesses

XRD was used for CuI samples to ensure their presence. By analyzing the pattern for both samples, peaks at 25, 30, 43, 50 and 52 correspond to CuI and it is aligned with the reference sample. Peaks around 43 and 50 are overlapping with Cu peaks and it is split into two peaks, one sharper than the other which indicate that copper is transforming into copper iodide. Moreover, the intensity of the thicker sample is higher which supports the claim that increasing the thickness increases the intensity of the peaks as well.

b. Electroless deposition technique

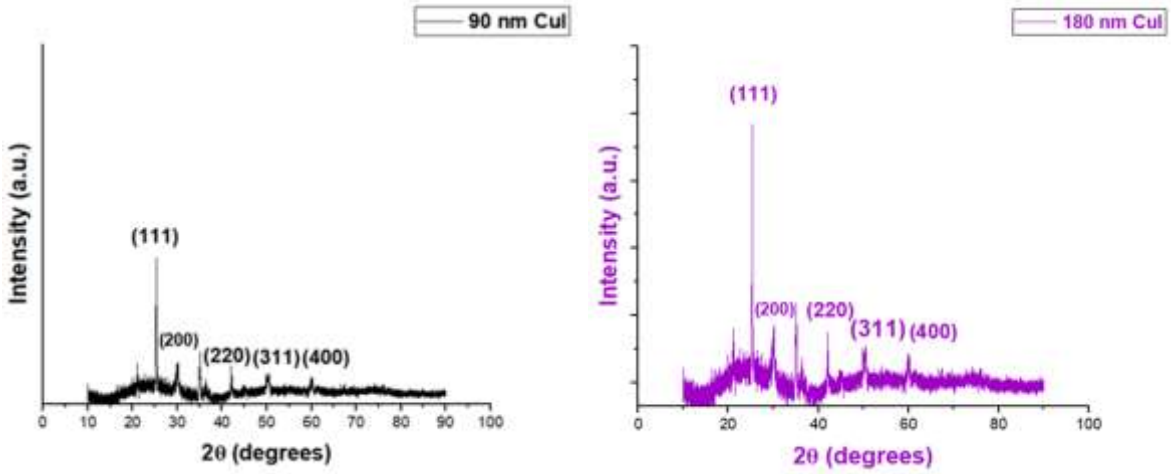

Figure (12): XRD pattern of CuI thin film

Repeatedly, for the samples prepared by the electroless deposition method, a profilometer was used to indicate their thickness and as expected the thickness of the samples has increased after the exposure to iodine vapor. The 40 nm sample has increased to 90 nm and the 96 nm sample has increased to 180 nm. These values are needed to calculate the volume.

Moreover, Xrd was used to ensure the presence of CuI in the sample. The same observation was noticed here as the previous sample. Peaks around 25, 30, 43 and 50 correspond to CuI. The intensity of the 90 nm CuI peaks is relatively weak when compared to the 180 nm CuI peaks which indicates that an increase in thickness contributes to an increase in peak intensities.

Table 2: Dimensions values of both substrates

Sample	Length (cm)	Width (cm)	Thickness (cm)	Volume (cm^3)
90 nm CuI	1	0.8	0.000009	0.0000072
180 nm CuI	1	0.7	0.000018	0.0000126

Table 2, represents the values of the length and width of both samples and by knowing the value of thickness, the volume is calculated. Thus, it was noticed here as well that the increase in thickness leads to higher volume. Concluding that 180 nm CuI has more diffusion of iodine through the thin film.

5. Synthesis of Copper Iodide Complexes

5.1 Introduction

The active layer of the solar cell is required to have long term optical and electrical stability. It is also required to have high photoelectric conversion efficiency and easy control over the band gap energy [22].

Moreover, for commercialization demands, the manufacturing cost of the photoabsorption layer must be satisfied. In this research study, 3,5-Dimethylpyridine is used as an absorbent material in the active layer.

5.2 Synthesis

CuI samples were placed inside a small vial which is inside a bigger one. 5-7 drops of 3,5-Dimethylpyridine liquid sample were placed inside the large vial and it was closed tightly. The reaction is kept for 24 hours.

5.3 Results

5.3.3 Thickness of the film

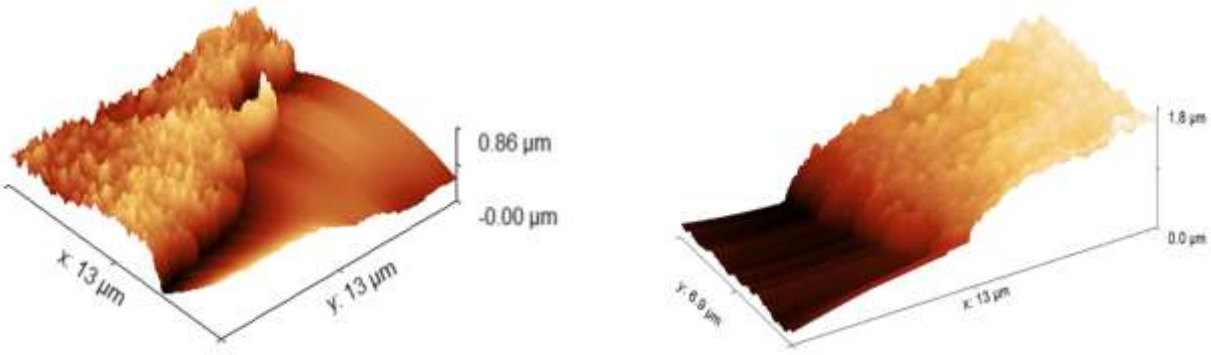

Figure (13): 3D AFM images of CuI-ligands

For this part, timing is important in order to take the necessary measurements because the ligand evaporates from the surface after one hour. Therefore, considering the time, the thickness of CuI-complex film is the only information taken from afm and it's useful to determine the volume.

As expected, the thickness increased significantly from 270 nm to 430 nm and for 160 nm, the thickness increased to 310 nm.

Table 3: Dimensions values

Sample	Length (cm)	Width (cm)	Thickness (cm)	Volume (cm^3)
310 nm CuI-complex	1	0.8	0.000031	0.0000248
430 nm CuI-complex	1	0.7	0.000043	0.0000301

The volume was calculated here as well to see how much the ligand is diffusing through the film and by knowing the values of the surface area and thickness it was shown that the thicker sample has a higher volume which indicates that the ligand is diffusing more.

6. Conclusion

In conclusion, the purpose of this project was to investigate the influence of the thickness on the surface morphology and roughness and to also calculate the volume which is an indication of how much iodine or ligand is diffusing through the film.

Moreover, two different methods have been used for the synthesis of metallic electrodes, thermal evaporator and electroless plating. By comparing both methods, samples obtained by thermal evaporator were stable and showed better results when analyzing their XRD patterns; however, this method is time consuming and the same thickness can be obtained within 3-5 minutes using the electroless plating method.

In addition, in terms of roughness the results show that the increase in thickness leads to more rough surfaces with high Sa and Sq values. In terms of the surface morphology, the increase in thickness leads to a more homogenous and well defined surface which indicates that the quality of crystallization improves. Finally, in terms of volume, it was indicated that the thicker samples have higher volume which means more diffusion of iodine and ligand into the film.

For future work, several additional steps can be added. For instance this project focused on three layers which is the metallic electrode , HTL and active layer. Perhaps adding ETL with suitable material and transparent electrodes can tell us more about the influence of thickness.
Moreover, two thicknesses were used only for this project, however in the future it would be better to study 4-5 different thicknesses to ensure that the results that we got are correct. Finally by knowing the volume, this can open new doors to different projects to find out about more undefined variables.

7. References

1. (No date) *Www.bp.com*. Available at: https://www.bp.com/content/dam/bp/business-sites/en/global/corporate/pdfs/energy-economics/statistical-review/bp-stats-review-2022-full-report.pdf (Accessed: September 19, 2022).
2. Mufutau Opeyemi, B. (2021) "Path to sustainable energy consumption: The possibility of substituting renewable energy for non-renewable energy," *Energy (Oxford, England)*, 228(120519), p. 120519. doi: 10.1016/j.energy.2021.120519.
3. Heintzenberg, J. and Rummukainen, M. (1993) "Airborne particles in snow," *Journal of glaciology*, 39(132), pp. 239–244. doi: 10.3189/s0022143000015896.
4. Miqael, A. (2022) *Solar Cell*, *Nevada Solar Group*. Available at: https://nevadasolargroup.com/solar-cell/ (Accessed: September 19, 2022).
5. Fazeli, H. (no date) *What would happen if we covered the Sahara Desert with solar panels?*, *Kcl.ac.uk*. Available at: https://blogs.kcl.ac.uk/sustainability/2021/08/what-would-happen-if-we-covered-the-sahara-desert-with-solar-panels/ (Accessed: September 19, 2022).
6. Green, M. A. (1993) "Silicon solar cells: evolution, high-efficiency design and efficiency enhancements," *Semiconductor science and technology*, 8(1), pp. 1–12. doi: 10.1088/0268-1242/8/1/001.
7. Mulvaney, D. (2014) "Solar's green dilemma," *IEEE spectrum*, 51(9), pp. 30–33. doi: 10.1109/mspec.2014.6882984.
8. Ahmed, M. I., Habib, A. and Javaid, S. S. (2015) "Perovskite solar cells: Potentials, challenges, and opportunities," *International journal of photoenergy*, 2015, pp. 1–13. doi: 10.1155/2015/592308.
9. Green, M. A. and Ho-Baillie, A. (2017) "Perovskite solar cells: The birth of a New Era in photovoltaics," *ACS energy letters*, 2(4), pp. 822–830. doi: 10.1021/acsenergylett.7b00137.
10. Stenberg, J. (no date) *Perovskite solar cells*, *Diva-portal.org*. Available at: http://www.diva-portal.org/smash/get/diva2:1117755/FULLTEXT02.pdf (Accessed: September 19, 2022).
11. Bashir, A. *et al.* (2020) "Interfaces and surfaces," in Awan, T. I., Bashir, A., and Tehseen, A. (eds.) *Chemistry of Nanomaterials*. Elsevier, pp. 51–87.
12. Kim, J. J. and Cha, S. H. (2002) "Optimized surface treatment of indium tin oxide (ITO) for copper electroless plating," *Japanese journal of applied physics (2008)*, 41(Part 2,11A), pp. L1269–L1271. doi: 10.1143/jjap.41.l1269.
13. Yamada, N., Ino, R. and Ninomiya, Y. (2016) "Truly transparent p-type γ-CuI thin films with high hole mobility," *Chemistry of materials: a publication of the American Chemical Society*, 28(14), pp. 4971–4981. doi: 10.1021/acs.chemmater.6b01358.
14. *AFM principle - how does an atomic force microscope work?* (no date) *Oxford Instruments*. Available at: https://afm.oxinst.com/outreach/how-does-an-afm-microscope-work (Accessed: September 19, 2022).

15. *X-ray diffraction for determining atomic and molecular structure* (2018) *Jove.com*. Available at: https://www.jove.com/v/10446/x-ray-diffraction (Accessed: September 19, 2022).
16. Nath, B. *et al.* (2022) "Role of electrodes on perovskite solar cells performance: A review," *ISSS journal of micro and smart systems*. doi: 10.1007/s41683-021-00089-y.
17. Chen, R. *et al.* (2022) "Rear electrode materials for perovskite solar cells," *Advanced functional materials*, 32(26), p. 2200651. doi: 10.1002/adfm.202200651.
18. Pydzińska-Białek, K., Nowaczyk, G. and Ziółek, M. (2022) "Complete perovskite solar cells with gold electrodes studied in the visible and near-infrared ranges," *Chemistry of materials: a publication of the American Chemical Society*, 34(14), pp. 6355–6366. doi: 10.1021/acs.chemmater.2c00845.
19. Tavakoli Dastjerdi, H. *et al.* (2020) "Cost-effective and semi-transparent PbS quantum dot solar cells using copper electrodes," *ACS applied materials & interfaces*, 12(1), pp. 818–825. doi: 10.1021/acsami.9b18487.
20. Li, S. *et al.* (2021) "A brief review of hole transporting materials commonly used in perovskite solar cells," *Rare metals*, 40(10), pp. 2712–2729. doi: 10.1007/s12598-020-01691-z.
21. Peng, W. *et al.* (2020) "Structure, binding energy and optoelectrical properties of p-type CuI thin films: The effects of thickness," *Applied surface science*, 502(144424), p. 144424. doi: 10.1016/j.apsusc.2019.144424.